Low-Temperature Anomalies of Two-Photon Absorption in In_2O_3 Nanocrystals Incorporated into PMMA Matrixes

I. V. Kityk*

Institute of Physics, J.Dlugosz University Czestochowa,Al.Armii Krajowej 13/15, Czestochowa, Poland

Qingsheng Liu, Zhaoyong Sun, and Jiye Fang*

Department of Chemistry and AMRI, University of New Orleans, New Orleans, Louisiana 70148, USA

Received: December 27, 2005; In Final Form: March 8, 2006

By using a method of two-photon absorption, it has been observed that monodisperse In_2O_3 nanocrystals (NCs) with sizes equal to ∼14−24 nm show significant increase of two-photon absorption at low temperatures. When $T = 40$ K, the two-photon absorption coefficients for low-sized samples drastically increase, whereas such enhancement for the samples with averaged sizes above ∼24 nm is not significant. The nondiagonal tensor components give one-order-less two-photon absorption values. A principal role in the observed dependences is played by interface nanolayers, demonstrating substantial contribution of nanoconfined effects. This phenomenon could only be observed in highly monodisperse NCs. Increase of the size distribution substantially suppresses the two-photon absorption observed. For the relatively large nanocrystals, the effects are comparable with those of the bulklike crystals. At the same time, the drastic increase at low temperatures may indicate a substantial role of the phonon subsystem.

1. Introduction

It has been a concern that nanocrystals (NCs) attract more interest in nonlinear optic and optoelectronic applications[1] due to the nanosized quantum-confinement effects. Such effects can be observed[2] when the samples possess definite sizes with a monodisperse distribution. To observe the quantum-confinement effects, there are crucial values of particle size and the size distribution. For semiconducting NCs, particles with a size larger than 8−9 nm are traditionally considered as "large-sized" samples.[3] In the case of "large particles", interfaces seem to be crucial, whereas the remaining bulklike background serves only as the assisting background necessary for keeping the nanosurfaces. It has been reported[4] that it would be an efficient way to observe the nonlinear optical (NLO) effect when semiconducting NCs were incorporated into the polymer matrixes due to the interfaces of NC−self as well as the borders surrounded by polymers.[5] For large-sized semiconducting NCs, it is crucial to consider the bulklike and near-surface states superposition to effectively contribute to the output of nonlinear optical susceptibilities.

It is usually believed that the quantum-confinement effects can only be determined when the size of semiconducting NCs reduces below 8−10 nm.[6] In such cases, **k**-space bulklike dispersion disappears and discrete excitonic-like nanolevels occur intra the energy gap.[7] For large-sized NCs, we have estimated that the typical thickness of bulklike behavior distributed by thin near-surface boundary interfaces is about 1.5−2.5 nm.

The quantum-confined boundary interfaces possessing bulklike as well as dotlike quantized excitonic properties can also be significant for different optical phenomena[8,9] and, particularly, for second- and third-order NLO investigation (both organic and inorganic ones) due to large charge density gradients determining high values of the NLO susceptibilities.[10,11] Reconstructed interface boundary sheets with thickness of 1.5−2.5 nm, separating the bulklike crystallites and surrounding the amorphous-like or disordered background, result in these features. Very often, this fact is neglected, which does not allow using it for further applications.

A principal parameter for the large-sized NC is a ratio between the thickness of the reconstructed boundary layer (sheet) and total effective diameter of the NC. Coexistence of bulklike long-range ordering possessing **k**-space dispersion, large effective mass, low carrier mobility, and quantum size-confined layers having substantial spectral blue-shift, opens a rare possibility to operate by electron parameters within the same crystallites.

As a separate topic, it is necessary to consider the role of different matrixes (polymers, glasses, and amorphous-like materials) in optoelectronic properties of NCs. The surrounding background plays a crucial role in application of the particular NC chromophores as materials for optoelectronic devices. An influence of the surrounding matrix on the band energy dispersion, effective masses, carrier mobility, values of the dipole moments, and corresponding optical susceptibilities requires more detailed considerations. Besides, the role of phonon subsystem may also give a contribution, particularly at low temperatures.[4]

As additional promising materials for such goals, one can choose the In_2O_3 semiconducting NCs. These NCs are perfect materials for transparent electrodes. Moreover, large second-order nonlinear optical susceptibilities were discovered on a border separating these films and the substrate. The main goal of this work is to study the influence of the nanocrystallite sizes on the two-photon absorption.

* Corresponding authors. i.kityk@ajd.czest.pl (I.V.K.); jfang1@uno.edu (J.F.).

10.1021/jp0575254 CCC: $33.50
Published on Web 04/20/2006

2. Experimental and Characterization Method

2.1. Synthesis of In_2O_3 Nanocrystals. In_2O_3 NCs were synthesized in a hot hexadecane solution under an argon stream by using a device described previously.[12] Typically, a proper amount of indium acetate, oleylamine, and oleic acid were introduced into hexadecane in a three-neck flask equipped with a condenser. All of the starting materials were employed as received from Aldrich without further purification. The reaction system was evacuated at room temperature for 15 min and, subsequently, at 110 °C for 15 min, respectively. TMNO was then added into this vigorously stirred mixture at 110 °C under an argon stream. The reaction temperature was further increased to 120 °C. After a reaction for 1 h under agitation and argon protection, the temperature was further increased to 290 °C at a rate of 10 °C/min for an additional 35 min of reflux. The products were cooled to room temperature by rapidly removing the heating source and isolated by adding a sufficient amount of ethanol and separating with centrifugation. After a posttreatment of size-selective precipitation, the monodisperse In_2O_3 NCs were stored in hexane or toluene.

2.2. Sample Preparation. To investigate various characteristics, these In_2O_3 NCs were self-assembled on TEM grids and on the surface of a single-crystalline Si wafer for morphological characterization by using a transmission electron microscope (JEOL 2010) and for phase identification by using an X-ray diffractometer (Philips X-pert system), respectively. Light scattering experiment was conducted on a DynaPro 99 molecular sizing instrument. To prepare the samples for nonlinear optical measurements, the solvent of hexane was dried under vacuum, and In_2O_3 NCs were redispersed into poly(methyl methacrylate)−chloroform (PMMA−chloroform) solution in a concentration of ~4.3% (by weight). Our previous investigations have shown that the PMMA matrixes due to their low polarizability do not disturb and change the degree of the NC monodispersion in the corresponding composites.[4]

2.3. Two-Photon Absorption. Generally, the two-photon absorption (TPA) is determined by an imaginary part of third-order optical susceptibility described by a fourth-rank polar tensor. The macroscopic susceptibility is related with microscopic hyperpolarizability by a relation:[13]

$$\chi_{ijkl} = L_i L_j L_k L_l \gamma_{ijkl} \tag{1}$$

where $L_{i,j,k,l}$ are i,j,k,lth local field Lorenz components, and γ_{ijkl} are microscopic third-order hyperpolarizabilities. For the simplified three-band model, the hyperpolarizability γ_{ijkl} is related to the principal microscopic parameters by an equation:

$$\gamma_{ijkl} \simeq \sum_k \frac{\vec{\mu}_i \vec{\mu}_j \Delta\vec{\mu}_k \Delta\vec{\mu}_l}{E_g^{\,3}} \tag{2}$$

where $\vec{\mu}_i$ is the ith component of transition dipole moment for optical transition between the levels, forming an efficient energy gap E_g, and $\Delta\vec{\mu}_l$ is the difference between the excited and ground dipole moments for the levels forming the efficient interband energy interval E_g; the contribution from the different points of the band structure are summarized and renormalized over the number of summated points k in the BZ. The dipole moments have two parts; a more strong electronic part, which is only slightly dependent on temperature, and a phonon part, which is very sensitive to occurrence of phonon modes, particularly at low temperatures near Debye temperatures. It is well-known that, near the Debye temperature, several phonon modes (so-called "soft" phonon modes) may have singular-like temperature dependences of the susceptibilities:

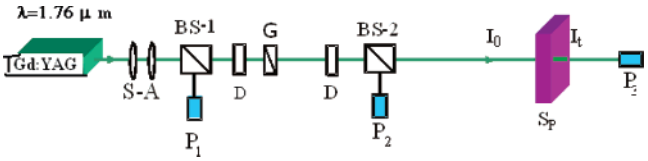

Figure 1. Principal setup for measurements of the NLO properties.

$$n_{ph} \approx |T - T_c|^{-\gamma} \tag{3}$$

where power parameter γ is strongly dependent on the type of the corresponding phonon mode condensation. In the refs 4 and 13, it was shown that, at low temperature, increase of the TPA may be caused by condensation of the low-frequency electron−phonon interactions. It is a main reason the susceptibilities, particularly optical ones, are dependent on the temperature.[4,13]

We have performed the TPA measurements by using a fundamental laser beam illumination of the pulsed Gd:YAG laser ($\lambda = 1.76$ μm) (pulse duration 10 ns, pulse power about 1 MW) (see Figure 1), which is transparent for the investigated samples. Average light power densities were varied up to 1.40 GW/cm^2. The sample temperature was monitored by a microthermobolometer chip with an accuracy up to 0.2 K. The highest local heating observed due to absorption of the sample did not exceed 0.8 K. The setup also allows a movement over the specimen's surface by the fundamental laser light beams. The beam profile sequence had a Gaussian-like shape with a half-width dispersion equal to about 78%. The laser power stability was maintained within 0.1%. The values of the TPA coefficients were determined from pump dependences of the transparency T using an expression:

$$T = 1 - \beta d I_p \tag{4}$$

where β is the evaluated TPA coefficient, d, sample thickness, and I_p, the power density of the pumping beam. The maximally achieved TPA values were achieved for parallel polarizations of the incident and output beams corresponding to diagonal tensor components of the β.

3. Results and Discussion

3.1. Size and Phase Verification. Parts a, b, c, and d of Figure 2 show transmission electron microscopic images of samples 1004B, 0925F, 0701004K, and 0913C, respectively, demonstrating high quality in morphology and narrow distribution in size. From these short-range close-packed patterns, it can be detected that the average diameters for four samples are about ~24.4 ± 1.1 nm, ~18.1 ± 0.9 nm, ~15.4 ± 0.9 nm, and ~13.5 ± 0.8 nm, respectively. The standard deviation of crystalline size for any of these samples was calculated as no larger than ~6%. To verify the size determination from TEM, we have also conducted light scattering measurement for three samples. Parts a, b, c, and d of Figure 3 present the radius distribution for four samples of In_2O_3 NCs. On the basis of light scattering measurements, the mean radii of 1004B, 0925F, 0701004K, and 0913C were calculated as 12.8, 8.9, 7.8, and 7.4 nm, respectively. These results are in good agreement with those from our TEM observation. For all of the four In_2O_3 samples, X-ray diffraction (XRD) investigation indicates a cubic phase because all of the detectable diffraction peaks in each pattern are indexed to those from body-center cubic In_2O_3 (ICDD PDF card no. 06-0416). The average sizes of crystallites

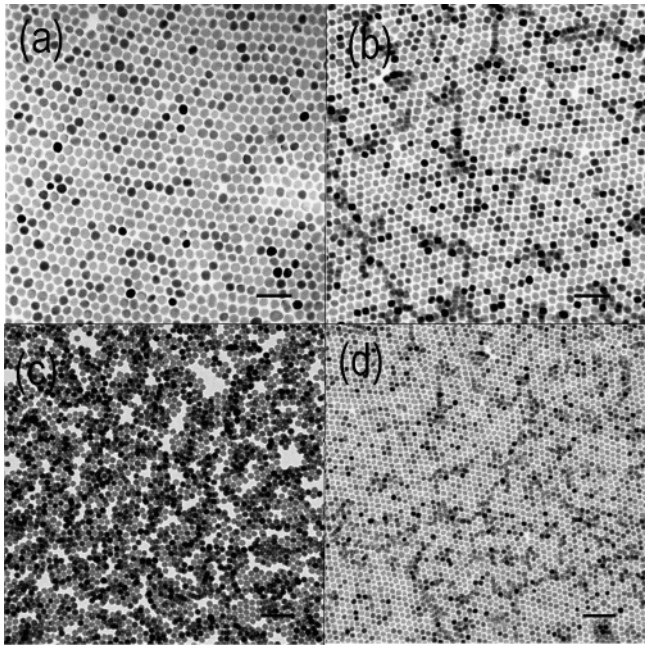

Figure 2. Transmission electron micrograph (TEM) images, recorded from (a) 1004B, (b) 0925F, (c) 0701004K, and (d) 0913C, respectively. Each bar presents 100 nm.

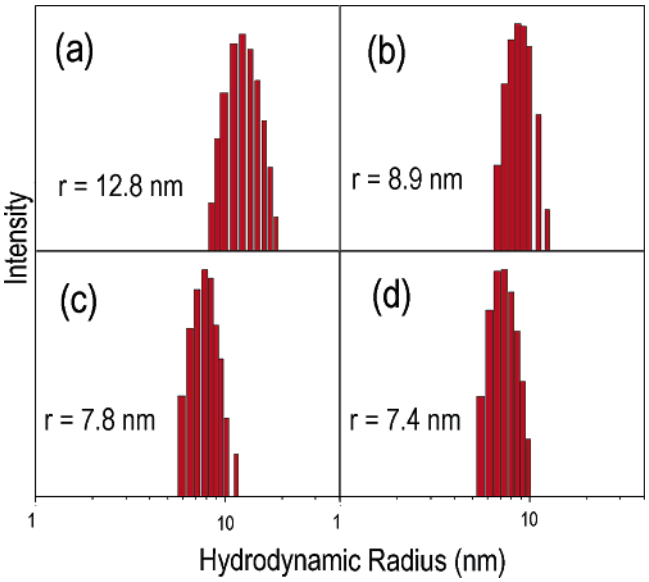

Figure 3. Crystalline size distributions of samples (a) 1004B, (b) 0925F, (c) 0701004K, and (d) 0913C.

for four samples, 22.9, 17.7, 15.2, and 13.2 nm, estimated by applying the Scherrer equation,[14] are close to those calculated from the TEM image (Figure 2d). As an example, the XRD pattern recorded from sample 0913C is demonstrated in Figure 4.

3.2. Nonlinear Optical Investigation and Role of Nanointerfaces. Figure 5 presents typical dependences of transparency versus intensity of fundamental Gd:YAG laser beams. One can clearly see that, with decreasing of temperature up to the liquid helium temperature, the bends in the transparency dependencies drastically increases. The relative precision of the transparency determination was equal to about 3%. In the TPA determination, inhomogeneity of the NC incorporation gives an error of ~4.5%. It exhibits that the bulklike samples possess the maximal changes of the transparency (at $T = 4.2$ K), which are at least a half order less. This may serve as an additional evidence of the principal role played by the nano-interfaces.

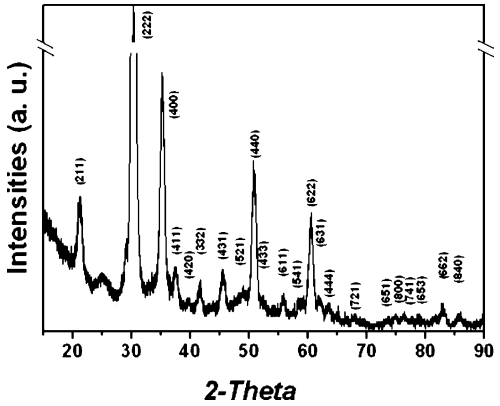

Figure 4. X-ray powder diffraction pattern of In_2O_3 sample 0913C.

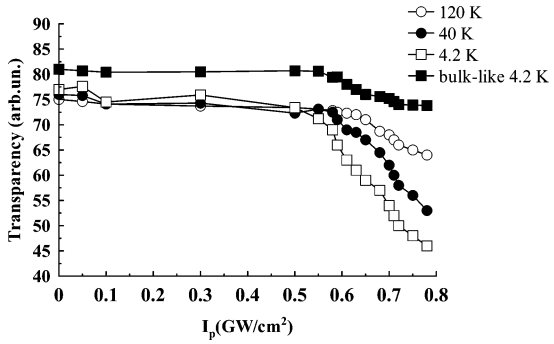

Figure 5. Intensity-dependent transparency of the In_2O_3 NCs incorporated into the PMMA with sizes equal to about 14 nm at different temperatures. For comparison, that of bulklike crystals is also presented.

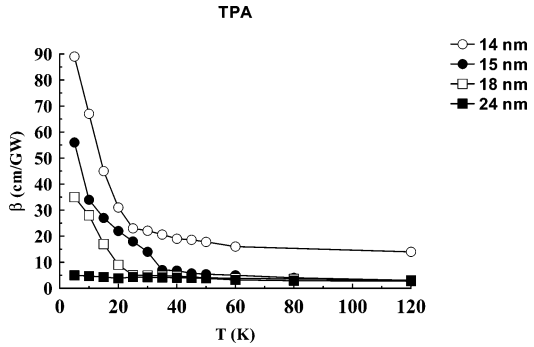

Figure 6. Temperature dependence of the TPA for the NCs incorporated into the PMMA matrixes.

Figure 6 demonstrates the results of the measured TPA diagonal tensor components β versus temperature, showing that a drastic increase of the corresponding TPA coefficients for the low-size samples occurs when the temperature is lower than 40 K. Nevertheless, such an enhancement is very insignificant for those samples with averaged sizes of ~24 nm or above. The nondiagonal tensor components give one-order-less TPA values. For the relatively large nanocrystallites, the effect is comparable with the bulklike crystals (i.e., it is very low). It is necessary to emphasize that the mixture of the NC possessing different sizes substantially suppresses the TPA. At the same time, the drastic increase at low temperatures may indicate a role of the phonon subsystem, which is more "sensitive" to temperature compared to the electronic subsystem.[15] A particular role for such effects may play the "condensation" of the appropriate anharmonic phonon modes near the Debye temperature, which was observed for several NCs.[4] The data obtained show a possibility of using the investigated NCs as promising materials for the optical limiting devices used in the different

apparatus. Generally, the value is substantially higher than that of the borate nanocrystallites doped by rare earths.[13]

It is important to add that these nanocomposites processed possess high technological stability, particularly with respect to external optical fields, temperature, and humidity. The maximal effect was observed for diagonal TPA tensor components corresponding to parallel polarizations of the incident and output beams. A specially performed experiment in the cooling−heating regime does not show a temperature hysteresis.

It is clear that a crucial role in the observed optical susceptibilities for the NC concerning optical and electronic properties is played by reconstructed interface sheets of the NC, which, following the data from electron microscopy and NMR studies, are of 1−3 nm in thickness. One can, therefore, expect the appearance of reconstructed near-surface structures possessing structural conformations corresponding to thermodynamically metastable (or even unstable) states.

Finally, it would be important to emphasize the drastic jump of the TPA between the NC with the sizes 14 and 15 nm. It may reflect the existence for these sizes of the critical nanosheet, which was independently manifested during the investigations of the In_2O_3 nano-interfaces.[16]

4. Conclusions

Experimental investigations of the two-photon absorption diagonal tensor components of the In_2O_3 nanocrystals versus temperature have been carried out. We have determined that, below 40 K, an enhancement of the corresponding two-photon absorption coefficients for the samples with low nanocrystal sizes (below 24 nm) occurred. The nondiagonal tensor components give one-order-less two-photon absorption values. For the relatively large nanocrystals, the effects are comparable with those of the bulklike crystals. It is necessary to emphasize that the mixture of the nanocrystals possessing different sizes does not give substantial contribution to this phenomenon. The data acquired demonstrate a possibility of using nanocrystals as promising materials for the optical limiting devices for various applications.

Acknowledgment. This work was supported by NSF CAREER Program (DMR-0449580), NSF NER program (DMI-0508412) and DARPA HR0011-05-1-0031.

References and Notes

(1) Komorowska, K.; Brasselet, S.; Dutier, G.; Ledoux, I.; Zyss, J.; Poulsen, L.; Jazdzyk, M.; Egelhaaf, H.-J.; Gierschner, J.; Hanak, M. *Chem. Phys.* **2005**, *318*, 12.

(2) Ahn, B. Y.; Seok, S. I.; Hong, S.-I.; Oh, J.-S.; Jung, H.-K.; Chung, W. J. *Opt. Mater*. **2006**, *28*, 374

(3) Kityk, I. V. *Semicond. Sci. Technol*. **2003**, *18*, 1001.

(4) (a) Kityk, I. V.; , *J. Non-Cryst. Solids* **2001**, *292*, 184. (b) Ebothé, J.; Kityk, I. V.; Fuks-Janczarek, I. *Appl. Surf. Sci*. **2006**, doi: http://dx.doi.org/10.1016/j.apsusc.2005.07.055.

(5) Kityk, I. V.; Sahraoui, B.; Ledoux-Rak, I.; Sallé, M.; Migalska-Zalas, A.; Kazuo, T.; Gorgues, A. *Mater. Sci. Eng. B* **2001**, *87*, 148.

(6) Hill, N. A.; Whaley, K. B. *Chem. Phys.* **1996**, *210*, 117.

(7) Ellert, C.; Schmidtr, M.; Reiners, T.; Haberland, H. *Z. Phys. D: At., Mol. Clusters* **1997**, *39*, 317.

(8) Horvath, Zs. J. *Curr. Appl. Phys.* **2006**, *6*, 145.

(9) (a) Nayak, J.; Sahu, S. N. *Physica E* **2005**, *30*, 107. (b) Migalska-Zalas, A.; Sofiani, Z.; Sahraoui, B.; Kityk, I. V.; Tkaczyk, S.; Yuvshenko, V.; Fillaut, J.-L.; Perruchon, J.; Muller, T. J. J. *J. Phys. Chem. B* **2004**, *108*, 14942.

(10) Shuan, K. Reports on Chemical Biophysics. In *Chin. Chem. Bull.* **2004**, 314.

(11) Mavi, H. S.; Prusty, S.; Shukla, A. K.; Abbi, S. C. *Opt. Commun*. **2003**, *226*, 405.

(12) Liu, Q.; Lu, W.; Ma, A.; Tang, V.; Lin, J.; Fang, J. *J. Am. Chem. Soc.* **2005**, *127*, 5276.

(13) Majchrowski, A.; Kityk, I. V.; Ebothe, J. *Phys. Status Solidi B* **2004**, *241*, 3047.

(14) Cullity, B. D. *Elements of X-ray Diffraction*, 2nd ed.; Addison-Wesley: Reading, MA, 1978.

(15) Zhu, K.-R.; Zhang, M.-S.; Chen, Q.; Z. Yin. *Phys. Lett. A* **2005**, *340*, 220.

(16) Ebothé, J.; Kityk, I. V.; El Hichou, A.; El Idrissi, B.; Addou, M.; Krasowski, J. *J. Vac. Sci. Technol., A* **2003**, *21*, 201.